

pubs.acs.org/est Article

# Breaking the Forever Bonds: Interface-Enhanced Superoxide Chemistry for Efficient PFOA Degradation

Wenbo You, Kejian Li, Qiuyue Ge, Yangyang Liu, Wei Wang, Haiping Xiong, Jianpeng Ao, Jilun Wang, Le Yang, Runbo Wang, Tingting Huang, Shiyi Wang, Huan Liu, Minbiao Ji, and Liwu Zhang\*



Cite This: Environ. Sci. Technol. 2025, 59, 19068-19080



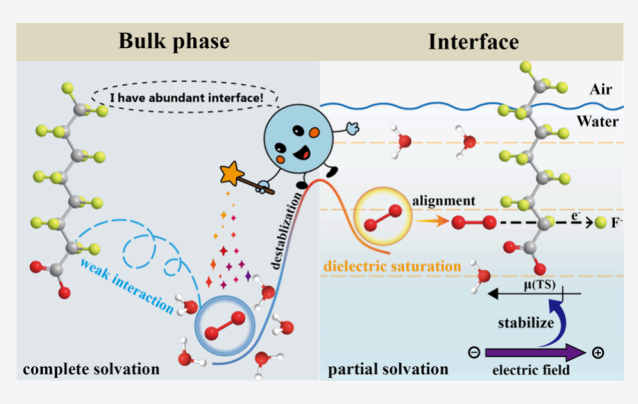
**ACCESS** I

Metrics & More

Article Recommendations

Supporting Information

**ABSTRACT:** The exceptional stability of carbon-fluorine (C-F) bonds in perfluorooctanoic acid (PFOA) presents a fundamental challenge in environmental remediation as traditional degradation methods struggle to break these bonds under mild conditions. Here, we demonstrate that the air-water interface in microdroplets can be strategically utilized to dramatically enhance PFOA ( $C_0 = 20 \text{ mg L}^{-1}$ ) degradation through a simple Fe(III)-Oxalate photochemical system, achieving complete destruction with 99% defluorination within 4 h at room temperature - a rate 2 orders of magnitude faster than conventional methods. Through comprehensive spectroscopic and computational investigations, we reveal that this remarkable enhancement stems from three synergistic interfacial effects: concentrated generation of superoxide radicals (O2 -) from earth-abundant Fe(III)-



Oxalate complexes, significantly enhanced O2" nucleophilicity due to disrupted solvation shells, and a strong interfacial electric field that catalyzes C-F bond activation. These molecular-level insights into interfacial chemistry not only provide an efficient and economical strategy for PFOA remediation but also establish a new paradigm for enhancing nucleophilic reactions in aqueous systems. Our findings highlight the transformative potential of air-water interfaces in activating traditionally inert chemical bonds, offering new opportunities for both environmental protection and chemical synthesis.

KEYWORDS: PFOA, microdroplet, air-water interface, photochemistry, superoxide radical

### **INTRODUCTION**

Per- and polyfluoroalkyl substances (PFASs) are synthetic chemicals extensively utilized by human society and contain at least one fully fluorinated methyl  $(-CF_3)$  or methylene  $(-CF_2-)$  group. Among the numerous PFAS compounds, perfluorooctanoic acid (PFOA) is particularly notorious, which has been widely used in industrial manufactures of firefighting foams, waterproofing materials, textiles, and personal care products over the past 60 years. 1-3 Unfortunately, given the escalating releases of PFOA, it has caused global concerns owing to its persistence, toxicity, and bioaccumulation, as well as the severe human health outcomes like cancer, immune system dysfunction, and developmental disorders.<sup>4,5</sup> A lot of remediation methods have emerged for PFOA treatment over recent decades. Typically, PFOA is physically extracted from polluted water by using active carbon adsorption, ion exchange, and high-pressure membrane technologies,6 and then the concentrated PFOA residues would be subjected to destructive treatment approaches like photochemistry, 7,8 electrochemistry, 9,10 sonochemistry, 11 photocatalysis, 12 plasma-based, and radiolytic processes. Most of these chemical treatment techniques rely on oxidative species (e.g., hydroxyl radical (OH), sulfate radical (SO<sub>4</sub>.-), and photogenerated hole

(h<sup>+</sup>)) or reductive species (e.g., hydrated electron (e<sub>ac</sub><sup>-</sup>)). However, traditional redox treatment approaches are generally inefficient for complete PFOA defluorination due to the challenges in cleaving highly stable C-F bonds (116 kcal/ mol). 15 Even though we have previously demonstrated that the air-water interface could enhance PFOA decomposition with reactive nitrogen species, the degradation efficiency was still not satisfactory, especially in large-scale applications. 16

The origin of the particular strength of the C-F bond is its high polarity. The electron density is substantially located at the fluorine atom. This leads to the unusual stability of C-F derived from the electrostatic attraction between  $C^{\delta'_+}$  and  $F^{\delta-}$ components, rather than the more classical electron pair sharing in the middle of a covalent bond. 17 It is therefore not surprising that conventional redox agents would struggle to homolytically cleave C-F bonds; injection or removal of one

Received: May 26, 2025 Revised: July 15, 2025 Accepted: August 19, 2025 Published: August 28, 2025





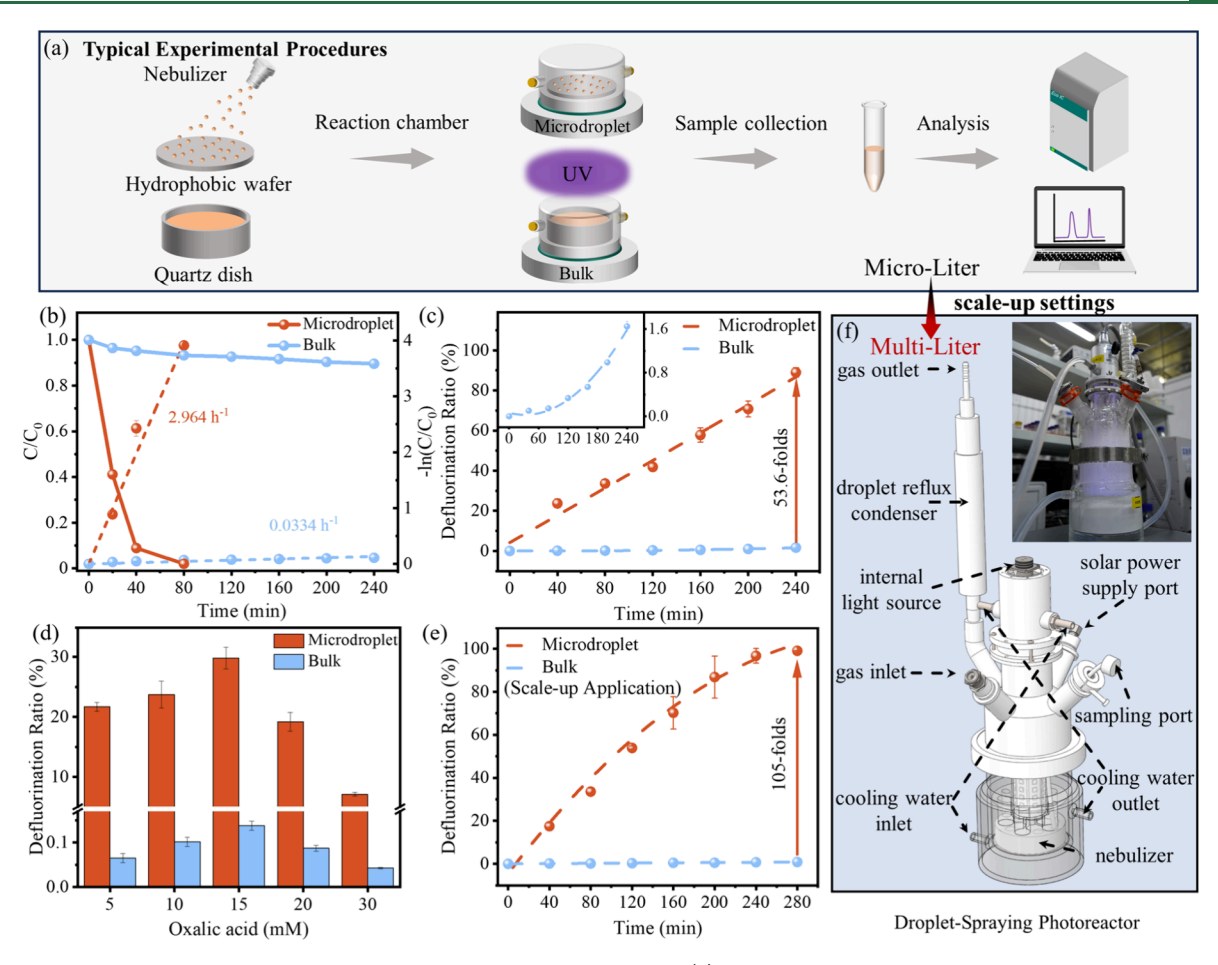


Figure 1. PFOA decomposition performances in microdroplets and bulk phase. (a) Schematic illustration of typical experimental procedures for microdroplet and bulk phase reaction; (b) time dependence of PFOA photochemical degradation and pseudo-first-order reaction kinetics fitting; (c) Defluorination ratio of PFOA in microdroplet and bulk phase; (d) impact of initial oxalic acid concentration on PFOA photochemical defluorination ([PFOA] =  $20 \text{ mg L}^{-1}$ , [Fe(III)] = 1 mM, reaction time = 40 min); (e) defluorination ratio of PFOA for scale-up applications; (f) scale-up instrumental setup of "Droplet-Spraying Photoreactor" (inlet: photograph of reactor in operation).

electron through a single electron transfer (SET) mechanism can only decrease the bond covalent character, which, however, is less prevalent over C-F bonding. Thereby, new chemical reactivity must be explored to break the C-F bond more efficiently. Superoxide radical (O2 -), with negative reduction potential  $(E_0(O_2/O_2^{-}) = -0.33 \text{ V})$ , is endowed with an additional electron within one of its  $\pi^*$  antibonding orbitals, which renders it a pronounced nucleophilic property. 18 It was reported that O2 is highly selective in the dehalogenation of electrophilic halogenated contaminants such as carbon tetrachloride and butyl bromide for their nucleophilic features. 18-21 This exceptional reactivity may arise from the sterically small and strongly electron-withdrawing nature of halogen atoms (X), which induces a significant positive charge density on the C-X carbon and a low-lying  $\sigma^*$  C-X antibonding orbital. In this regard, as an electron-rich nucleophile,  $O_2^{-}$  is expected to smoothly overlap the  $\sigma^*$  C-X orbital with its oxygen lone pairs, and the halogen moiety contributes stabilization to the negative charge brought by O2 -. Consequently, such substitution-dehalogenation, as proceeding via an electron-pair transfer mechanism, could be a preferable way over the conventional redox-based process. While most of these reactions were carried out with -Cl or -Br substituted compounds, there were some early reports that PFOA defluorination can also be achieved in similar

mechanisms. In 2014, Watts's group reported that approximately 68% of PFOA removal in the  $\rm H_2O_2$  propagation systems could be attributed to the  $\rm O_2^{-.22}$  These researchers also noted a strong solvent effect on the  $\rm O_2^{-}$  reactivity. Later, Guo et al. found that  $\rm O_2^{-}$  was insignificantly scavenged by coexistent contaminants compared to OH, rendering  $\rm O_2^{-}$  highly available for PFOA removal in the ozonation processes. Furthermore, Bai et al. pointed out that the C–F bond cleavage by  $\rm O_2^{-}$  through bimolecular nucleophilic substitution ( $\rm S_N2$ ) pathway is thermodynamically favorable, with  $\Delta G_R^{-0} = -4.09~\rm kcal~mol^{-1}.^{24}$ 

Despite these pioneering studies, the mechanism of  $O_2$  induced C–F cleavage is still not completely resolved and under debate. One open question is that the full potential of  $O_2$  nucleophilicity can be largely untapped in aqueous systems due to two major issues: (1) quick disproportionation upon interaction with protons, and (2) rapid stabilization through hydrogen bondings with water. The latter implies that a breaking of existing hydrogen bonds in the  $O_2$  -( $H_2O$ ) $_n$  complex is needed in order to permit an effective nucleophilic attack by  $O_2$ . To maintain the nucleophilicity, the use of costly ionic liquids, spatial confinement, or phase-transfer catalysts is often required. These limitations have led to low catalyst turnovers and restricted the practical application of  $O_2$  in PFOA remediation. It came to our attention that recent

advances in microdroplet chemistry have revealed remarkable rate accelerations  $(10^3-10^6 \text{ times})$  and even enabled previously unfeasible reactions. <sup>30–37</sup> Of particular relevance, theoretical studies predict enhanced nucleophilicity of O2 at air-water interfaces, with its redox potential decreased by 0.32 V compared to bulk water. 38-40 Since the interfacial ordered water molecules cannot participate as an efficient hydrogen bond donor, 41 O2 will not be stabilized by hydrogen bonding. This phenomenon diminishes to the  $S_N2$  transition state (TS) because the S<sub>N</sub>2 adduct possesses more dispersed charges, and the -F moiety holds four lone pairs tightly, which are reluctant to get involved in hydrogen bond interactions. Additionally, the strong electric field at the microdroplets' surface may further contribute to the alignment of the O2 with C-F bonds. 42 So we can expect a decrease in S<sub>N</sub>2 activation energy while an increase in exothermicity at the air-water interface. However, this theoretical prediction has not been experimentally validated or exploited for practical applications.

In the present paper, we are motivated to explore the possibility that microdroplets and the associated air-water interface might offer a more favorable environment than the bulk phase for "unlocking" the intrinsic nucleophilicity of O2. for C-F bond breaking. PFOA decomposition was investigated with photochemically generated O<sub>2</sub> from Fe(III)-Oxalate chelates. Our results suggest that the microdropletbased approach achieved nearly complete PFOA ( $C_0 = 20 \text{ mg}$ L<sup>-1</sup>) destruction with 99% defluorination within 4 h at room temperature, a performance that significantly surpasses conventional methods. Through comprehensive mechanistic investigations using advanced spectroscopic techniques and theoretical calculations, we uncover how the unique physicochemical environment at the air-water interface synergistically promotes O2 generation, extends its lifetime, and facilitates its reaction with PFOA. Most importantly, we successfully translated this fundamental breakthrough into a practical application by developing a scale-up "Droplet-Spraying Photoreactor" capable of treating PFOA-contaminated water at the liter scale. This work not only provides new fundamental insights into interfacial chemistry but also offers a promising solution to one of the most pressing environmental challenges of our time.

### MATERIALS AND METHODS

Typical experimental procedures are depicted in Figure 1a. Microdroplets were generated using a custom-built nebulizer and deposited onto a preprepared superhydrophobic quartz wafer, which exhibited water contact angles of  $142 \pm 1^{\circ}$  (as shown in Figure S1). The wafer was positioned approximately 3 cm away from the outlet of the nebulizer, and the solution in the nebulizer (composed of 1 mM FeCl<sub>3</sub>, 10 mM H<sub>2</sub>C<sub>2</sub>O<sub>4</sub>, and 20 mg  $L^{-1}$  PFOA, pH = 1.84) was thoroughly mixed prior to spraying. As illustrated in Figure S2a, the diameters of microdroplets deposited on the wafer were predominantly ranged from 130 to 240  $\mu m$  with an average size of 188  $\mu m$ . The wafer was then placed into a custom-designed reaction chamber (Figure S3a) under high relative humidity conditions (RH > 90%). The chamber was irradiated by a low-pressure mercury lamp centered at 254 nm with a power density of 2.55 mW cm<sup>-2</sup>. Due to the strict control of low temperature and high relative humidity, the size of microdroplets experienced negligible changes during the reaction (Figure S2). 43,44 For comparison, the bulk phase reaction was performed in a miniature quartz Petri dish in the same reaction chamber

under identical irradiation conditions, containing 3 mL of solution with a thickness of  $\sim$ 1 cm (Figure S3b). The absorption of PFOA by a superhydrophobic wafer or quartz dish was minimal, as shown in Figure S4.

For scale-up reactions, a novel "Droplet-Spraying Photoreactor" was fabricated by the authors. A standard 1.5 L volume of solution (composed of 1 mM FeCl<sub>3</sub>, 10 mM  $\rm H_2C_2O_4$ , and 20 mg  $\rm L^{-1}$  PFOA) was introduced into the reactor. The photochemical reactions within the reactor were driven by a 180 W LED light source (255  $\pm$  15 nm narrow band irradiation) and cooled with 15 °C circulating water. Microdroplets were formed and regenerated by an ultrasonically nebulizer (95 W) located at the bottom of the reactor. Bulk phase reaction was conducted without operation of the ultrasonic nebulizer. Aliquots of the solution were taken at time intervals of 40 min for up to 280 min. Detailed descriptions of the scale-up reaction settings are provided in Supporting Information (SI).

All control experiments were conducted following typical experimental procedures with the reaction time fixed at 40 min. Solution pH was adjusted with 0.1 M H<sub>2</sub>SO<sub>4</sub> and 0.1 M NH<sub>3</sub>·H<sub>2</sub>O to investigate the effects of pH. In order to explore the role of microdroplet size on photochemical decomposition of PFOA, the average diameter of the microdroplets <500  $\mu$ m was controlled by adjusting the number of sprays of the nebulizer. Single spray events produced small droplets that collided and merged on the superhydrophobic wafer, gradually forming larger droplets of various sizes. Droplets >500 μm were directly dispensed onto the superhydrophobic substrate using a 2.5 µL micropipette. Figure S5 displays representative micrographs of microdroplets with distinct average sizes. After predetermined time intervals, samples were collected and quantitatively diluted using 0.01 M HCl containing 5 vol % TBA to inhibit iron precipitation and cease the reaction. 45 The obtained samples were filtered using a 0.45  $\mu$ m polycarbonate membrane before analysis, and all experiments were performed in triplicate. The descriptions of analytic methods, stimulated Raman spectroscopy, interfacial electric field, and transient absorption spectroscopy measurements, and density functional theory calculations are provided in the SI.

### ■ RESULTS AND DISCUSSION

Enhanced PFOA Decomposition in Microdroplets. Fe(III)-Oxalate chelates are common composites in natural waters and have been reported to be effective photo-Fenton catalysts. Under light irradiation, the complexes can undergo a ligand-to-metal charge transfer (LMCT) process to generate reactive oxygen species (ROS, typically O2 and OH) (eqs 1-8). Hence, we explored the PFOA (20 mg L<sup>-1</sup>, the concentration is comparable to that found in an air station using aqueous fire-fighting foam)46 photodegradation efficiency by using Fe(III)-Oxalate chelates photochemistry in both microdroplet and bulk phase (as shown in Figure 1a, for typical experimental procedures). Figure 1b illustrates the substantial enhancement of PFOA removal efficiency in microdroplets compared to the bulk phase: after 80 min of UV light irradiation, the microdroplet reaction achieved almost complete PFOA removal with a degradation efficiency of 98.02%. In stark contrast, the bulk phase counterpart only yielded 7% PFOA degradation after the same duration, with a removal efficiency of merely 10.43% even after 4 h. Pseudofirst-order reaction kinetic fitting showed that the PFOA degradation rate constant was 2.964 h<sup>-1</sup> in microdroplets,

which was about 88.74 times faster than that in the bulk phase counterpart (0.0334 h<sup>-1</sup>, Figure 1b dashed lines). Defluorination ratio was adopted to further evaluate PFOA elimination performances, as the strong persistence of PFOA mainly resulted from its highly stable C-F bonds. According to Figure 1c, the defluorination ratio continuously increased with time. After 40 min, the defluorination efficiency in microdroplets reached 23.72%, 235 times larger than the bulk phase reaction (0.101%). After 240 min of irradiation, the final defluorination ratio reached 88.49 and 1.65% in microdroplets and the bulk phase counterpart, respectively. To clarify the individual contributions of UV irradiation, Fe(III)-Oxalate catalyst, and microdroplets, a series of control experiments was conducted (Table S1). The results showed that neither microdroplets alone (not detected), UV alone (0.03%), nor the combination of UV and microdroplets without Fe(III)-Oxalate (0.06%) can lead to appreciable defluorination after 4 h, indicating that the high efficiency is attainable only when all three components are present and highlighting the unique advantage of microdroplets in promoting PFOA photochemical decomposition. 47-55

[Fe(III)(
$$C_2O_4$$
)3]<sup>3-</sup> + hv  $k = 0.04 \text{ M}^{-1} \text{ s}^{-1}$   
 $\rightarrow [\text{Fe}(\text{II})(C_2O_4)2]^{2-} + C_2O_4^{-}$  (1)

$$C_2O_4^- \to CO_2^- + CO_2 \quad k = 2 \times 10^6 \,\text{M}^{-1} \,\text{s}^{-1}$$
 (2)

$$CO_2^- + O_2 \rightarrow CO_2 + O_2^- \quad k = 6.5 \times 10^9 \,\mathrm{M}^{-1} \,\mathrm{s}^{-1}$$
 (3)

$$O_2^{-} + H^+ \rightarrow HO_2^- \quad k = 10^{4.8} \,\mathrm{M}^{-1} \,\mathrm{s}^{-1}$$
 (4)

$$HO_2' + HO_2' \rightarrow H_2O_2 + O_2 \quad k = 8.3 \times 10^5 \,\mathrm{M}^{-1} \,\mathrm{s}^{-1}$$
 (5)

Fe(II) + H<sub>2</sub>O<sub>2</sub> 
$$k = 63 \text{ M}^{-1} \text{ s}^{-1}$$
  
 $\rightarrow \text{Fe}(\text{III}) + \text{OH}^{-} + \cdot \text{OH}$  (6)

$$C_2O_4^{2-} + \cdot OH$$
  $k = 7.7 \times 10^6 \text{ M}^{-1} \text{ s}^{-1}$   
 $\rightarrow CO_2 + CO_2^{-} + OH^{-}$  (7)

$$\cdot_{\text{OH}}^{+\text{H}_2\text{O}_2} \rightarrow \text{O}_2^{-}/\text{HO}_2^{-} \quad k = 3.3 \times 10^7 \,\text{M}^{-1} \,\text{s}^{-1} + \text{H}_2\text{O}$$
 (8)

Fe(II) + ·OH + H<sup>+</sup> 
$$k = 4.3 \times 10^8 \,\text{M}^{-1} \,\text{s}^{-1}$$
  
 $\rightarrow \text{Fe(III)} + \text{H}_2\text{O}$  (9)

$$CO_2^- + [Fe(III)(C_2O_4)_3]^{3-}$$
  $k = 10^9 \sim 10^{10}$   
 $\rightarrow Fe(II) + CO_2 + 3C_2O_4^{2-}$   $M^{-1} s^{-1}$  (10)

Additionally, the defluorination ratio of PFOA was found to be first increased and then decreased with increasing the initial concentrations of oxalic acid (Figure 1d). The highest defluorination ratio (29.78%) was observed in the presence of 15 mM  $\rm H_2C_2O_4$  after 40 min of irradiation. The volcanotype variation trend could be explained by the dependence of speciation of Fe(III)-Oxalate chelates on the concentration ratio of  $\rm H_2C_2O_4$  to Fe(III). The majority of Fe(III)-containing species would shift from  $[\rm Fe(C_2O_4)]^+$  and  $[\rm Fe(OH)]^{2+}$  to  $[\rm Fe(C_2O_4)_2]^-$  and  $[\rm Fe(C_2O_4)_3]^{3-}$  as  $\rm H_2C_2O_4$  concentrations increased.  $^{56}$   $[\rm Fe(C_2O_4)_2]^-$  and  $[\rm Fe(C_2O_4)_3]^{3-}$  exhibit stronger

photochemical reactivity compared to  $[Fe(C_2O_4)]^+$  and  $[Fe(OH)]^{2+}$ , thereby resulting in the faster PFOA defluorination rate at higher H<sub>2</sub>C<sub>2</sub>O<sub>4</sub> concentrations. However, excessive H<sub>2</sub>C<sub>2</sub>O<sub>4</sub> (>15 mM) had a detrimental effect on PFOA defluorination. This was likely because surplus H<sub>2</sub>C<sub>2</sub>O<sub>4</sub> scavenged OH (eq 7), and thus inhibited O2 generation through eq 8, and retarded Fe(III) recycling (eq 9) for continuous photo-Fenton reactions. In addition, PFOA degradation showed high sensitivity to pH, with the highest defluorination ratio (23.22% after 40 min of irradiation) observed at pH = 2 (Figure S8). High concentrations of H<sub>2</sub>C<sub>2</sub>O<sub>4</sub> would lead to a more acidic solution, with pH values of 1.99, 1.84, 1.74, 1.69, and 1.56 for 5, 10, 15, 20, and 30 mM H<sub>2</sub>C<sub>2</sub>O<sub>4</sub>, respectively. The lower pH accelerated O<sub>2</sub>. disproportionation with H<sup>+</sup> (eqs 4 and 5). When pH rose above 3, Fe(III) began to precipitate, which in turn terminated the photochemical activity of the Fe(III)-Oxalate complex. The precipitation also disrupted the coordination between Fe(III) and the departing F atom, an interaction that may play a potential role in activating the C-F bond through Lewis acid catalysis.<sup>57</sup> As a result, the overall efficiency of PFOA defluorination declined sharply under basic conditions.

Further investigations were conducted to evaluate the influences of initial PFOA concentration and real water matrices on photochemical defluorination of PFOA. The defluorination ratios increased with decreasing initial concentrations of PFOA in both microdroplets and bulk phase systems, suggesting that the photochemical processes mediated by Fe(III)-oxalate complex are particularly advantageous for PFOA elimination at lower concentrations (Figure S9). Besides, the detected defluorination ratios of PFOA in various actual water matrices were also higher in microdroplets than in bulk solutions, confirming the feasibility of using microdroplets for PFOA defluorination in natural environments (Figure S10).

Scale-Up Applications. The aforementioned findings collectively suggest that microdroplets can substantially improve the photochemical degradation of PFOA. However, these experiments are conducted at small scales (microliter level). To facilitate scale-up applications, we have extended our work to the design of a "droplet-Spraying Photoreactor" aimed at treating multiliter quantities of PFOA-contaminated wastewater. Figures 1f and S5 present the instrumental design and setup. In this advanced system, microdroplets can be continuously produced by an ultrasonic nebulizer at the bottom of the reactor and diffuse within the ring-shaped column outside the immersion well. The thickness of this ringshaped column is 30 mm (50 mm ID, 110 mm OD) to ensure that the LED light source located in the immersion well can sufficiently irradiate the droplet zone. After condensation on walls, droplets can be directed back to the bottom of the reactor for recycling and respraying. As shown in Figure 1e, for a standard 1.5 L solution (20 mg L<sup>-1</sup> PFOA in 1 mM FeCl<sub>3</sub> and 10 mM H<sub>2</sub>C<sub>2</sub>O<sub>4</sub>), the photoreactor achieved nearly complete defluorination (99.05%) within 280 min. This rate was 120 times faster than that in the bulk phase reaction (0.82%). When the light source was off, the defluorination ratio significantly decreased, only 0.11% with spraying and 0.08% without spraying droplets (Table S2). This indicates that PFOA is difficult to degrade solely through the energetic cavities generated by ultrasound and is instead primarily degraded through the ROS produced by photochemical processes of Fe(III)-Oxalate. Additionally, the defluorination

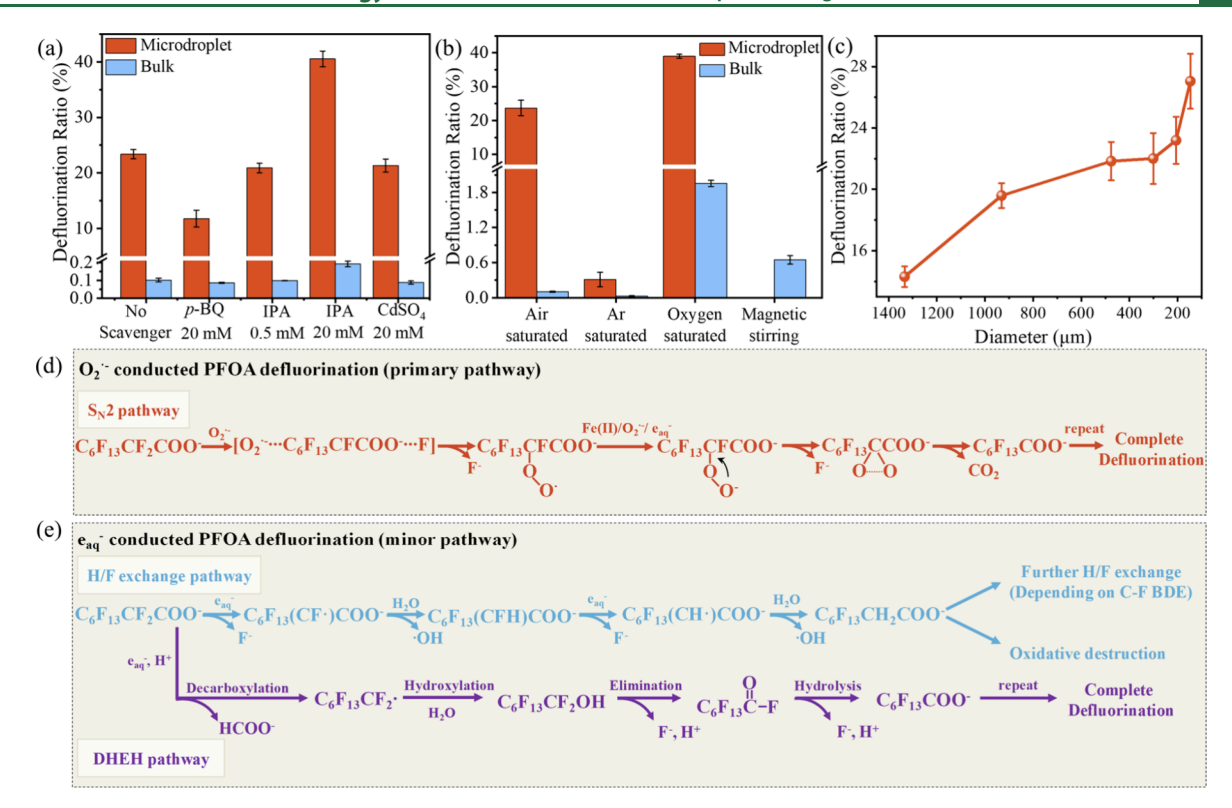


Figure 2. Reaction pathways investigation. Impacts of (a) ROS and  $e_{aq}^-$  scavengers, (b) reaction atmosphere, and (c) droplet size on PFOA photochemical defluorination ([PFOA] = 20 mg L<sup>-1</sup>, [Fe(III)] = 1 mM, [H<sub>2</sub>C<sub>2</sub>O<sub>4</sub>] = 10 mM, reaction time = 40 min). Reaction pathways of PFOA degradation induced by (d)  $O_2^-$ , and (e)  $e_{aq}^-$  in microdroplets.

efficiency obtained in the scale-up reaction exceeds that observed in the typical experimental procedure at the microliter level (88.49%, Figure 1c). The improved performance is likely due to the creation of charged, and smaller droplets ( $<10~\mu m$ ) by the ultrasound atomization compared to that deposited on a hydrophobic wafer ( $\sim188~\mu m$ , Figure S2). The interfacial charges may alter the hydration enthalpy of the ROS, while a smaller size ensures the droplet features a larger air—water interface, which is critical in modulating the generation and reactivity of ROS, as explored in subsequent sections.

Identification of Dominant ROS Responsible for PFOA Decomposition. Radical quenching experiments were performed to investigate the ROS responsible for PFOA degradation. As displayed in Figure 2a, the PFOA defluorination efficiency was significantly inhibited with the addition of 20 mM p-benzoquinone (p-BQ), a typical scavenger of O2-, indicating the pivotal role of O2- in PFOA elimination. The defluorination was almost completely suppressed under a high-purity Ar atmosphere, while the continuous supply of high-purity O2 and magnetic stirring evidently increased the defluorination ratio (Figure 2b). These results confirmed that the presence of O2 indeed participated in PFOA photochemical decomposition in the dominant form of  $O_2$ . The introduction of 0.5 mM isopropanol (IPA) resulted in a slight decrease in defluorination efficiency from 23.37% to 20.91%, suggesting that ·OH played a relatively insignificant role in PFOA decomposition, consistent with previous reports. 61-63 An unexpected increase in the defluorination ratio to 40.52% was observed when IPA concentration was elevated to 20 mM. Such anomalies were also reported in other O<sub>2</sub> involved halogenated pollutants

treatment processes,  $^{20,64,65}$  which may underscore the nuanced phenomenon of the solvation effect on  $O_2$ .

Hydrated electron,  $e_{aq}^{-}$ , can also be generated in our system, either by Fe(III)-Oxalate through charge-transfer-to-solvent (CTTS) process, <sup>66</sup> or by electrolysis of H<sub>2</sub>O in the presence of interfacial electric field. <sup>67,68</sup> To investigate the decomposition of PFOA by e<sub>aq</sub>-, electron quenching experiments were conducted using CdSO<sub>4</sub> as a specific scavenger of  $e_{aq}^-$  ( $k = 6.4 \times 10^{10} \text{ L mol}^{-1} \text{ s}^{-1}$ ).<sup>69</sup> As shown in Figure 2a, PFOA defluorination with the addition of 20 mM CdSO<sub>4</sub> was weakly inhibited (from 23.37 to 21.81%) compared with that in the presence of 20 mM p-BQ (from 23.37 to 11.75%), which indicates that  $e_{aq}^{-}$  is less responsible for PFOA degradation in this reaction system. This can be explained by the low quantum yield of eag through Fe(III)-oxalate CTTS process (0.05), and extremely slow kinetics for water electrolysis at the air-water interface. As Zhou et al. have quantitatively elucidated, only ~1 of 65,000 H<sub>2</sub>O molecules at the interface can be converted to  $H_2O_2$  and  $e_{aq}^-$  per second, with a maximum  $e_{aq}^-$  generation rate of 15.4 nmol  $m^{-2}$  min<sup>-1</sup> (assuming the stoichiometric ratio of  $e_{aq}^-$  to  $H_2O_2$  is 2:1).<sup>70</sup> Moreover,  $e_{aq}^-$  only preferred anoxic and basic conditions;  $e_{aq}^$ generated in current system can be substantially consumed by Fe(III), O<sub>2</sub> and H<sup>+</sup> rather than for defluorination, with the corresponding rate constants of  $k = 6.0 \times 10^{10}$ ,  $1.9 \times 10^{10}$ , and  $2.3 \times 10^{10}$  M<sup>-1</sup> s<sup>-1</sup>, <sup>71</sup>, <sup>72</sup> which are at least 3 orders of magnitude higher than that for  $e_{aq}^-$  and PFOA ( $k = 1.7 \pm 0.5$  $\times$  10<sup>7</sup> M<sup>-1</sup> s<sup>-1</sup>). <sup>73</sup> Consequently, while  $e_{aq}^-$  could contribute to the reductive degradation of PFOA in the current system, its impact was very limited.

Previous studies also suggested that Fe(III) could be complexed with PFOA and participate in the PFOA photo-

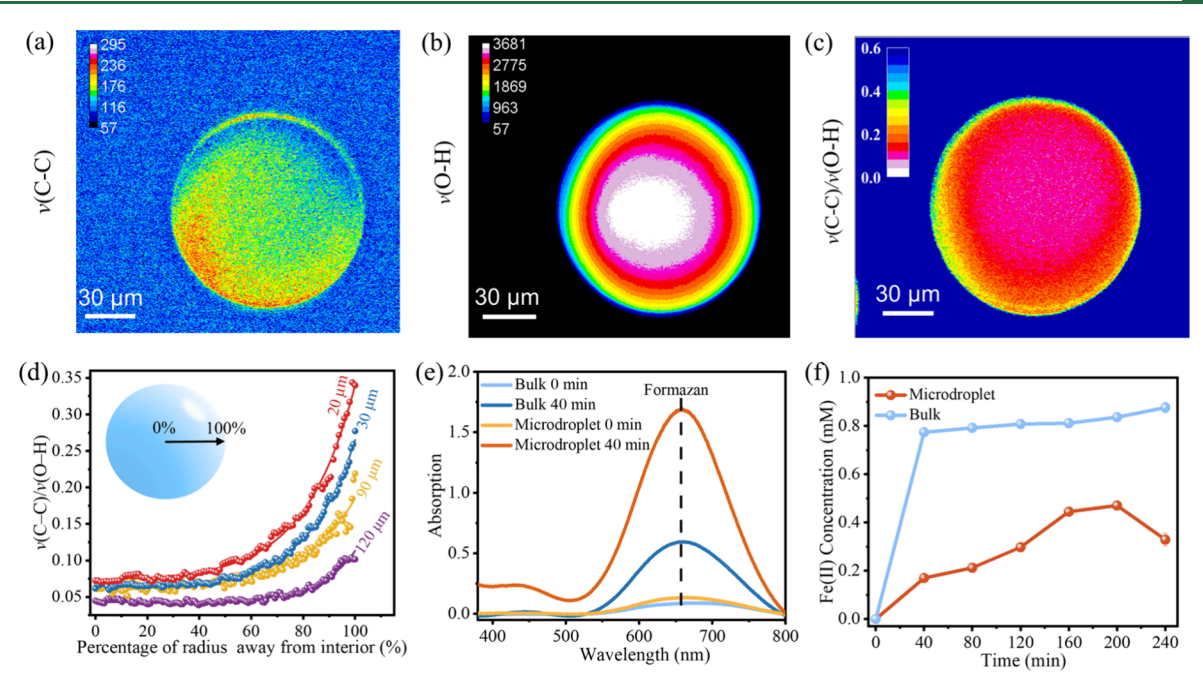


Figure 3. Concentration enrichment and enhanced  $O_2$  generation at microdroplet air—water interface. SRS spectra of (a)  $\nu(C-C)$  of  $C_2O_4^{2-}$ , (b)  $\nu(O-H)$  of  $H_2O$  and (c) calculated  $\nu(C-C)/\nu(O-H)$  in a 120  $\mu$ m microdroplet. (d) The intensity ratio of  $\nu(C-C)/\nu(O-H)$  as percentage of radius away from the microdroplets interior (droplet size: 20, 30, 90, and 120  $\mu$ m); (e) UV—vis absorption spectra of formazan, and (f) Time dependence of Fe(II) concentration in microdroplet and bulk phase.

degradation through the LMCT process. However, in the presence of excess oxalic acid, the Fe(III) would predominantly form Fe(III)-Oxalate chelates rather than Fe(III)-PFOA complexes. The preference can be attributed to the equilibrium constant of Fe(III)-PFOA complexes ( $10^{3.89}$ ) is lower by 3 orders of magnitude compared to that of Fe(III)-Oxalate chelates ( $3.9 \times 10^7$ ). Besides, the photochemical process of Fe(III)-Oxalate complexes could generate  $CO_2^-$ , which has a redox potential of  $-1.9 \, \text{eV}^{77}$  and has been proved to cleave C–Cl bonds. However, due to the rapid reaction between  $CO_2^-$  and  $O_2$  ( $k=6.5 \times 10^9 \, \text{M}^{-1} \, \text{s}^{-1}$ ), the generated  $CO_2^-$  would rapidly transform to  $O_2^-$  in the presence of  $O_2$ . Therefore, the roles of Fe(III)-PFOA complexes and  $CO_2^-$  in PFOA photodegradation were negligible.

Overall PFOA Degradation Pathways in Microdroplets. HPLC-MS/MS analysis illustrated that the degradation of PFOA was accompanied by the formation of short-chain perfluoroalkyl carboxylic acids (PFCAs) containing 2–7 carbon atoms, such as perfluorohexanoic acid (PFHxA) and perfluorobutanoic acid (PFBA), as depicted in Figure S11. The production of the short-chain PFCAs exhibited an initial increase, followed by a subsequent decrease, indicative of a stepwise degradation process for PFOA and its degradation intermediates. Based on the detected degradation intermediates and insights from radical quenching experiments, we propose that the degradation of PFOA primarily follows the pathways outlined below:

The PFOA decomposition would initiate with an  $S_N^2$  process, where  $O_2$  acts as the nucleophile and attacks the  $\alpha$ -C atom, whose C–F bond dissociation energy (BDE) has been reported to be the lowest on PFOA (107.2  $\pm$  0.4 kcal mol<sup>-1</sup>). This step leads to the formation of an  $S_N^2$  adduct  $[O_2$  ····  $C_6F_{13}$  CFCOO ···· F], followed by a concerted cleavage of the C–F bond and formation of a peroxy radical

 $(C_6F_{13}CF(O-O^{\circ})COO^{-})$  (eq 11).<sup>24</sup> The peroxy radical is an excellent electron acceptor, which can be smoothly reduced by means of single electron transfer from the various reducing species present in the reaction medium (Fe(II),  $O_2^{--}$ , and  $e_{aq}^{--}$ ) to generate peroxy anion  $(C_6F_{13}CF(O-O^-)COO^-)$ . The oxyanion on the terminal of the peroxy group is nucleophilic due to the filled nonbonding orbital, and can further interact with the empty  $\sigma^*$  orbital of the second C–F bond, leading to the C-F cleavage and generation of a three-membered cyclic intermediate. Such cyclic intermediate features a high ring strain, which can be readily released by homolytic cleavage of the O–O bond (BDE < 45 kcal/mol), 80,81 and coupled with decarboxylation of the peroxy group in the form of CO<sub>2</sub>. This process results in the production of one fewer -CF<sub>2</sub>- unit (in this stage, perfluoroheptanoic acid) compared to its parent compounds and is considered to be the primary mechanism for PFOA chain shortening without the involvement of other ROS. The generated short-chain PFCAs would repeat the above process, ultimately achieving complete decomposition. The schematic diagram of the overall degradation mechanism is present in Figure 2d.

$$O_{2}^{-} + C_{6}F_{13}CF_{2}COO^{-}$$

$$\stackrel{S_{N}^{2}}{\longleftrightarrow} [O_{2}^{-}\cdots C_{6}F_{13}CFCOO^{-}\cdots F]$$

$$\leftrightarrow C_{6}F_{13}CF(O - O\cdot)COO^{-} + F^{-}$$
(11)

Additionally, the formation of less fluorinated fluorotelomer carboxylate species (FTCAs, Figure S12) indicated that the  $e_{aq}^-$  involved reductive defluorination-hydration pathway also existed. PFOA destruction pathways by  $e_{aq}^-$ -assisted H/F exchange or decarboxylation—hydroxylation—elimination—hydrolysis (DHEH) mechanism has been extensively studied and reviewed (Figure 2e). Additionally, H/F exchange products, for example,  $C_6F_{13}CH_2COOH$ , can be oxidatively decomposed by OH for chain shortening, which might

elucidate the role of OH as demonstrated in ROS scavenging experiments. A recent study has also proposed a novel  $e_{aq}^{-}$ -induced "two-carbon shortening" process for the degradation of low-concentration PFOA in water droplets.<sup>84</sup> However, given the unimportant role of  $e_{aq}^{-}$  and its limited efficacy in treating short fluorocarbon chains (Figure 2a), a mechanistic investigation into these unfavorable pathways is beyond the scope of this study; instead, priority is given to clarifying the mechanism of the PFOA removal enhancement by  $O_2^{-}$ .

Mechanism Study for Rate Acceleration in Microdroplets. As an anionic surfactant, PFOA tends to accumulate at the air-water interface due to the intrinsic amphipathy. Here we found that the introduction of cetyltrimethylammonium bromide (CTAB, cationic surfactant) enhanced the defluorination ratio, while the addition of sodium dodecyl sulfate (SDS, anionic surfactant) showed a negative effect on PFOA defluorination (Figure S13). The converse effects might be because CTAB improved PFOA concentration enrichment at the water surface due to the electrostatic attraction between the oppositely charged molecules, as observed also in ref 86, while SDS suppressed the PFOA interfacial enrichment. Besides, as shown in Figure 2c, the photochemical defluorination ratio was significantly improved as the microdroplet size decreased from around 1350 to 150  $\mu$ m. The impacts of CTAB and SDS suggest that PFOA photodegradation primarily occurs at the air-water interface, and the microdroplet size effects verify the important role of the air-water interface in PFOA photodegradation. Hence, investigating the potential roles of the microdroplet air-water interface is crucial, which might predominantly involve the following three factors that synergistically augment the collision frequency of reactants within the confined interfacial space and decrease the reaction

Increased O<sub>2</sub><sup>--</sup> Generation at the Air–Water Interface. Previously, Jungwirth and co-workers reported that highly polarizable ions, such as oxalate anions, would preferentially accumulate at the air–water interface due to the polarization by the interfacial asymmetric water dipoles. Studies based on molecular dynamic simulation also suggest that there is a minimum free energy at the interfacial Gibbs dividing surface, indicating a pronounced surface affinity of solutes to the air—water interface. In this study, we experimentally analyzed the interfacial concentration enrichment of oxalate anions by Stimulated Raman Spectroscopy (SRS) measurements.

As shown in Figures 3a-c and S12, the oxalate concentration at the air-water interface, represented by the peak intensity ratio of v(C-C) to v(O-H) with the O-H of the H<sub>2</sub>O molecule as internal standard, is considerably higher than that in the microdroplet interior. This disparity becomes more pronounced (2.3–4.7 folds) as the droplet size decreased from 120 to 30  $\mu$ m (Figures 3d and S15), indicating a significant surface excess of oxalate anions, particularly in smaller droplets. Although Fe(III) cations may not inherently exhibit surface affinity due to their poor polarizability,<sup>87</sup> they can be dragged to the subsurface by the Coulomb force of the negatively charged oxalate and PFOA anions on the surface, resulting in a substantially higher concentration of Fe(III)-Oxalate chelates in the interfacial region. Besides, it is worth noting that the availability of dissolved oxygen (DO) at the air-water interface of microdroplets can exceed 300 mg/L, which is remarkably higher compared to the bulk solution (~8 mg/L). Under such abundant DO conditions, higher concentrations of Fe(III)-Oxalate are associated with increased

 $O_2$  generation, consequently resulting in more effective defluorination of PFOA (Figure S16).

To further analyze the disparity in O<sub>2</sub> generation between microdroplets and the bulk phase, O2 was semiquantitatively analyzed by the nitro blue tetrazolium (NBT) detection method. The reaction product between NBT and O<sub>2</sub>, formazan, was extracted and quantified by using UV-vis absorption spectroscopy. Figure 3e shows that the absorbance of formazan in microdroplets is approximately 4 times higher than that in the bulk phase counterpart, demonstrating that more of the O2 was generated in microdroplets. In addition, OH (the subsequent product of O2 -) was also quantificationally analyzed by benzoic acid oxidation, 91 and results showed that ·OH generation was about 10 times higher in microdroplets than that in the bulk phase system (Figure S17). These results suggest that the interfacial concentration enrichment of Fe(III)-Oxalate complexes and highly efficient O<sub>2</sub> accessibility made the interfacial photochemical ROS generation far beyond the bulk phase system. In the bulk phase, O<sub>2</sub> production is not only limited by the uniform distribution of Fe(III)-Oxalate complex, but also by the scarcity of DO, which can even alter the fate of CO<sub>2</sub><sup>--</sup> (the precursor for O2 -): CO2 is a powerful reducing agent and exhibits comparable reaction rates toward O2 and Fe(III) (with rate constants of  $k_{\rm O2} = 6.5 \times 10^9$  and  $k_{\rm Fe(III)} = 10^9 \sim 10^{10} \, \rm M^{-1}$  s<sup>-1</sup>, eqs 3 and 10). <sup>49,55</sup> The absence of sufficient O<sub>2</sub> would result in an undesired pathway in which CO<sub>2</sub> depletes Fe(III) and generates large amounts of Fe(II) in bulk phase in a short reaction time (as depicted in Figure 3f); in contrast, CO<sub>2</sub> can more easily interact with  $O_2$  at the air—water interface (eq 3), leading to substantial generation of O<sub>2</sub>.— within microdroplets.

Enhanced O<sub>2</sub> Reactivity at the Air—Water Interface. It is noteworthy that the observed 10<sup>2</sup>~10<sup>3</sup> acceleration on defluorination in microdroplets cannot be solely attributed to the increased ROS generation or O2 availability. This is supported by the observations that the augmentation of Fe(III)-Oxalate concentration in bulk solution (Figure S16) or O<sub>2</sub> availability (Figure 2b) only leads to a moderate increase in reaction rates. Indeed, the rate of an  $S_N 2$  reaction is directly related to the effectiveness of the nucleophilicity, which is strongly dependent on the degree of solvation. As O<sub>2</sub> is generated in the aqueous phase, solvents are intimately involved in the reaction process, and the ion-dipole interactions first produce  $O_2^-$ - $(H_2O)_n$  association complexes. This is related to a decrease in O2 free energy prior to any intrinsic chemical barriers of orbital overlap in the  $S_N$ 2 process. On the other hand, the TS of S<sub>N</sub>2 adducts can also be solvated by water from the point of view of thermal equilibrium, which must in turn compensate for the desolvation energy of  $O_2$  in the activation process—although this aspect has been frequently overlooked in most cases. An estimation of how solvents preferentially solvate reactants and TS must be made in order to judge the rate acceleration at the air-water interface.

As the reaction transferred from the bulk phase to the air—water interface, the relative modification in solvation energy can be quite different from reactants to TS, depending on their specific structures. One paramount factor is the molecular charge density, given that the interactions between solvents and solutes are typically the result of electrostatic forces. The rate-determining step of  $O_2$ —induced defluorination is the negatively charged nucleophile of  $O_2$ —to attack the C–F carbon to give  $S_N2$  adducts  $[O_2$ — $\cdots$  $C_6F_{13}CFCOO$ — $\cdots$ F]. The

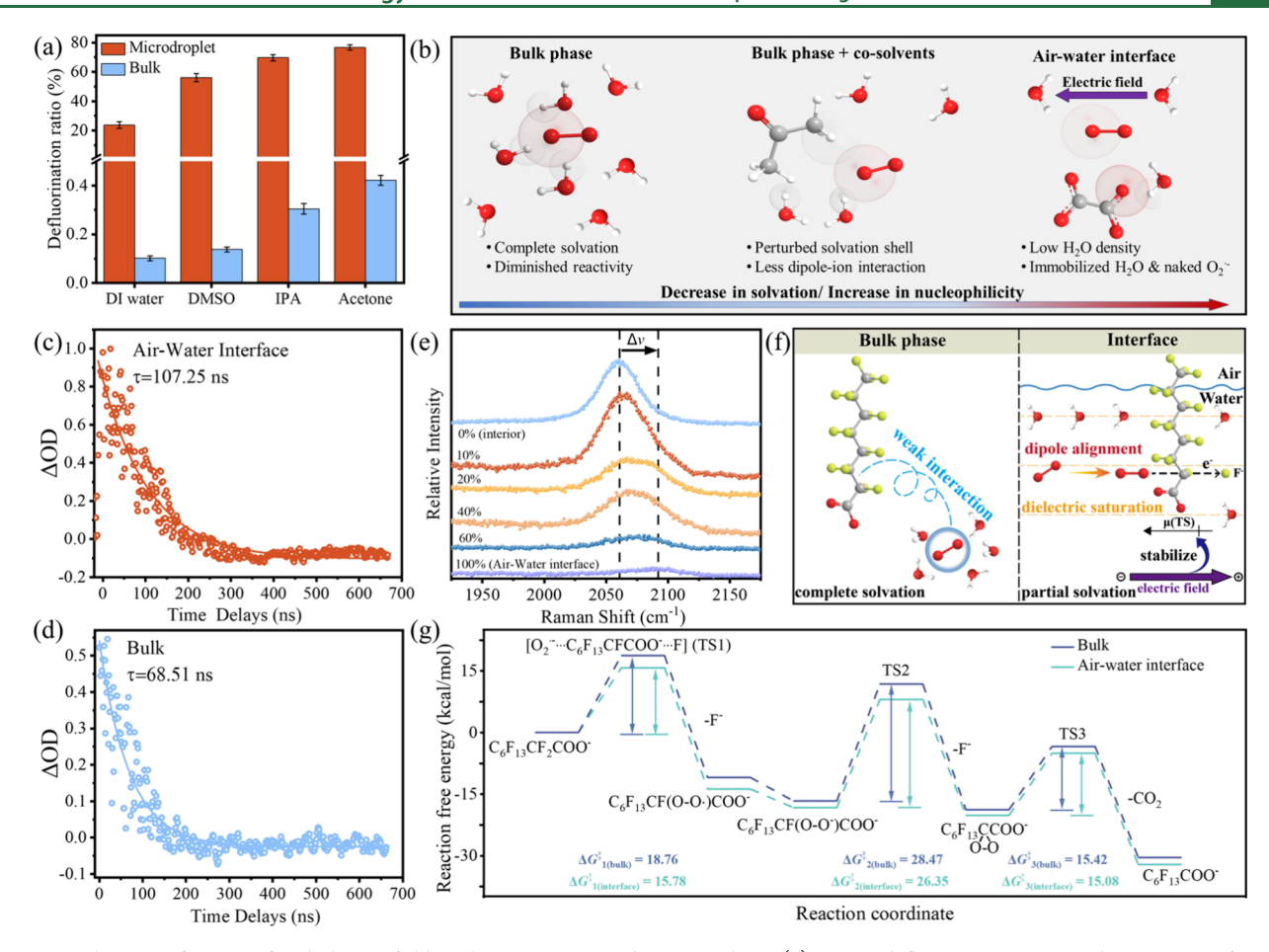


Figure 4. Solvation effect, interfacial electric field, and reaction energy barrier analysis. (a) PFOA defluorination ratio in the presence of various low-polarity solvent ([PFOA] = 20 mg L<sup>-1</sup>, [Fe(III)] = 1 mM, [H<sub>2</sub>C<sub>2</sub>O<sub>4</sub>] = 10 mM, reaction time = 40 min); (b) scheme of solvation states of  $O_2$ <sup>--</sup> under different reaction scenarios; nanosecond transient adsorption spectra of  $O_2$ <sup>--</sup> at (c) air—water interface and (d) bulk phase; (e) Raman spectra of  $\nu(C \equiv N)$  at different regions of microdroplet with size of 50  $\mu$ m; (f) scheme of mechanisms for the accelerated PFOA degradation at the air—water interface. The direction of the electric field is defined according to the convention used in the Gaussian package; (e) energy profiles for PFOA degradation processes conducted by  $O_2$ <sup>--</sup> in bulk solution and at the air—water interface. Red, white, gray, and green spheres in Figure b,f denote  $O_2$ ,  $O_2$ , and  $O_2$ ,  $O_2$ ,

charge localized in O2- can be strongly stabilized by water through ion-dipole interactions and hydrogen bonding. Such stabilization would be less prevalent for the [O2 -- ··· C<sub>6</sub>F<sub>13</sub>CFCOO-···F] in TS, as the charge of O<sub>2</sub>- is diffused over  $[O-C-F]^-$  atoms and thus  $[O_2^-\cdots C_6F_{13}CFCOO^-\cdots F]$  is less polar. This hydration difference makes the reactivity of O<sub>2</sub> diminish in water while contributing to the observed extremely high activation energy in the bulk phase. In contrast, solvents with low dielectric constant may fail to solvate O2. well, making  $O_2$  more reactive;  $[O_2$   $\cdots$   $C_6F_{13}CFCOO$   $\cdots$  F] is less in need of solvation due to charge dispersion, which implies a lower decrease in hydration enthalpy of TS compared to that of reactants, and so the net reaction would be faster. Therefore, we investigated the solvation effects of O<sub>2</sub><sup>--</sup> through introducing dimethyl sulfoxide (DMSO), isopropanol (IPA), and acetone with a concentration of 1 M into the pristine reaction medium (DI water). These cosolvents assisted in perturbing the solvation shells of O2- and reduced the solvation number of water. Meanwhile, owing to their larger molecular size and less acidic hydrogen (C-H or alcoholic O-H), these low-polarity solvents are relatively poor electron-pair acceptors (EPA) to accommodate O2 - (as illustrated in Figure 4b). Consequently, the dipole-ion interactions between the solvents and the O<sub>2</sub> anions weakened, which led to a decrease

in the hydration enthalpy of the  ${\rm O_2}^-$ . According to Figure 4a, the defluorination ratio of PFOA in microdroplets after 40 min photoirradiation was improved in the order of acetone (76.68%) > IPA (69.65%) > DMSO (56.16%) > DI water (23.71%), approximately in reverse order of their dielectric constants (78.0, 47.0, 19.9, and 21.0 for DI water, DMSO, IPA, and acetone respectively). Especially in the presence of 1 M aprotic solvent of acetone, a remarkable defluorination ratio of 76.68% was achieved, which is greater than almost all previous reports. The shift in IPA and acetone can be explained by the specific interaction of hydrogen bonding between IPA and  ${\rm O_2}^-$ . The energy required to disrupt hydrogen bonding adds to the activation energy in IPA.

We propose that the environment at the air—water interface could be closely analogous to those low-polarity solvents, as they both have *structure breaker* properties similar to those of the  $O_2^-$  solvation shells and are less efficient at solvating the  $O_2^-$  charges. Air—water interface is characterized by low water density and an asymmetric hydrogen bonding network, which intuitively reduces the degree of solvation of  $O_2^-$  especially for  $O_2^-$  located on the water surface, they are partially solvated and partially exposed to the air, thereby the interaction between  $O_2^-$  and interfacial water molecules is dramatically weakened, leading to almost naked  $O_2^-$  for

nucleophilic reaction. This is evidenced by a very recent work employing molecular dynamics simulation, wherein O<sub>2</sub> is found to stay on the droplet surface with a relatively higher energy level, forming only 1~2 weak hydrogen bonds with interfacial H<sub>2</sub>O compared to 4 hydrogen bonds in the bulk phase.<sup>94</sup> Moreover, electric fields at the air-water interface can reach as high as MV/cm (in the present case, 86.1 MV/ cm). 95-97 The electric field can not only catalyze reactions directly; it can also lead to dielectric saturation at the airwater interface, 60 where the dipole moments of water molecules become preferentially immobilized along the direction of the electric field, as justified by the decrease of local dielectric constant from 78.0 (bulk phase value) to 2.1 at the interface.  $^{98}$  In this case, water would undergo structure increase and is not able to reorient its dipoles to solvate the O2 anion. This effect could be more significant in the presence of a high ionic concentration at the surface of microdroplets (as depicted by SRS data in Figure 3a-d), in which scenario water molecules are tightly packed around charged ions of Fe(III) and oxalate as their hydration shells. Consequently, water loses its dipolar characteristic to interact with the developing charge when O<sub>2</sub> is created at the airwater interface, and the O2 is partially solvated and thus more reactive than in the bulk phase (as shown in Figure 4b). Bulk water, on the other hand, can rapidly respond to any charge fluctuations and heavily stabilize O2 -. This is confirmed by transient absorption spectroscopy (TAS) measurements (Figure 4c,d). Due to the incomplete solvation shell of  $O_2$ , the protonation-induced O2 disproportionation (eqs 4 and 5) is retarded at the air—water interface. The half-life span  $(\tau)$  of O<sub>2</sub> at the air-water interface reaches 107.25 ns, nearly twice as long as the bulk phase value of 68.51 ns. All these observations pointed to the fact that the O2 generated at the air-water interface is more reactive and has a longer lifetime for nucleophilic reaction with PFOA compared to the bulk phase counterpart.

Catalytic Role of the Interfacial Electric Field. Microdroplet chemistry studies revealed the presence of a strong and oriented electric field on the air—water interface, which may arise from the nonuniformly distributed ions and the broken symmetry of the neat water surface. The interfacial electric field can significantly impact molecule spectroscopy (such as Stark Effect) and facilitate electron transfer and redox reaction, thus influencing reaction free energy and impacting chemical reaction rates. Here, a confocal micro-Raman spectrometer was employed to directly measure the interfacial electric field in microdroplets based on the Stark vibrational effect. Too, 101 C≡N was chosen as the vibrational probe for its large dipole moment (~3D) to maximize the interaction with the electric field.

In a 50  $\mu$ m diameter microdroplet, the obvious blue shift of the Raman peak of  $\nu(C \equiv N)$  was observed as measured from microdroplet interior (2060.8 cm<sup>-1</sup>) to the interfacial region (2091.2 cm<sup>-1</sup>), corresponding to an electric field strength of 86.1 MV/cm (Figure 4e). Additionally, the electric field strength became stronger with decreasing microdroplet size (Figure S18). Such a high interfacial electric field is capable of influencing the chemical reactivity of  $S_N2$  defluorination, which is stereochemically constrained and requires the transfer of an electron pair from the nucleophile to the leaving group. <sup>104</sup> In the absence of an electric field, there is no external constraint, the distribution of PFOA and  $O_2$  is random, and it is difficult for  $O_2$  to attack the backside  $\alpha$ -carbon atom on PFOA to

interact with the  $\sigma^*$  antibonding orbital of the C-F bond. In the electric field present case, the polarized C-F would exhibit a large axial preference.  $^{105}$  C-F and  $^{105}$  are forced to align along the direction of the electric field due to the strong charge-dipole interactions for binding. The interfacial electric field thereby served as a tweezer that fixed the reagents to be prepared for S<sub>N</sub>2 displacement. 42 As such, even though the direction of the electric field may fluctuate significantly, as to be Lorentzian distributed at the air-water interface, 106 one could expect the reaction axis "O-C-F" would synchronously align along the axis of the external field in space (as exemplified in Figure 4f). This collinear configuration substantially compensated for the negative activation entropy for the S<sub>N</sub>2 mechanism, and allowed the electric field to maximally polarize the C-F bond at the given moment to push the electron pair in O<sub>2</sub> toward the terminal fluorine atom, thus intensifying the intermolecular bonding between the  ${\rm O_2}^-$  and electrophilic lphacarbon. Moreover, electrostatic theory allows us to qualitatively predict the external stabilization/destabilization effect of the electric field according to eq 12:99

$$\Delta \Delta E = 4.8 \overrightarrow{F} \cdot \Delta \overrightarrow{\mu} \text{ (kcal/mol)}$$
 (12)

The term  $\Delta \Delta E$  represents the stabilization energy difference between reactants and the TS under the electric field  $\vec{F}$  (V/Å), while  $\Delta \overrightarrow{\mu}$  denotes the dipole moment change (in Debye) along the reaction coordinate. 99 The polarized C-F bond and elongated geometry of the S<sub>N</sub>2 adduct would lead to an increased dipole moment in the TS, which is oriented from F toward O due to the charge transfer toward the more electronegative leaving group. In this case, vectors of  $\vec{F}$  and  $\Delta \overrightarrow{\mu}$  are relatively opposite to each other, thus pointing to a negative value of  $\Delta\Delta E$  that indicated a greater stabilization of the electric field on TS as compared to that of the ground state reactant, and thereby demonstrating an overall catalytic effect of the electric field on the reaction (Figure 4f). To demonstrate the validity of our proposals, a DFT calculation was carried out to compare the reaction free energy for O2induced PFOA degradation between the bulk phase and the air-water interface. As shown in Figure 4g, the C-F cleavage steps exhibited the highest activation energies of  $\Delta G^{\ddagger}_{1(\text{bulk})}$  = 18.76 kcal/mol and  $\Delta G^{\ddagger}_{2(bulk)} = 28.47$  kcal/mol in the bulk phase. In comparison, the same reaction steps that proceeded at the air-water interface are more barrierless with  $\Delta G^{\ddagger}_{1(\text{interface})} = 15.78 \text{ kcal/mol} \text{ and } \Delta G^{\ddagger}_{2(\text{interface})} = 26.35$ kcal/mol, predicting the rate constants of approximately 35-150 times higher than those in the bulk phase based on the Eyring equations. 107 This enhancement is in a level of agreement with our experimental observation of an 88.74fold increase in the pseudo-first-order rate constant, as fitted in Figure 1b. The elimination of the second F is more challenging, which could be due to the steric hindrance of the three-membered ring configuration that inhibited the oxyanion from aligning with the  $\sigma^*$  orbital of the residual C–F bond. Compared with defluorination steps, the decarboxylation step experienced relatively small energy barriers of 15.42 and 15.08 kcal/mol for bulk and interface. As this step involved the homolytic cleavage of O-O and C-C bonds, no significant charge reorganization occurred during the process. Consequently, the kinetic advantages of solvent effect on the decarboxylation step at the interface were limited, with the reaction energy barrier merely reduced by 0.34 kcal/mol,

practically through the catalytic role of the electric field. Overall, DFT calculation indicates that O2 experienced significantly lower energy barriers to get to the stabilized TS1 and TS2 by 2.98 and 2.12 kcal/mol, respectively, leading to accelerated PFOA defluorination at the air-water interface in microdroplets.

## ENVIRONMENTAL IMPLICATIONS

This work presents a fundamental breakthrough in PFOA remediation by harnessing the unique properties of air-water interfaces in microdroplets, demonstrating degradation rates 2 orders of magnitude faster than conventional bulk-phase treatments. Our mechanistic investigations reveal three synergistic factors driving this exceptional performance: enhanced O2 generation at the interface, dramatically improved O2 reactivity due to weakened solvation effects, and the catalytic role of the strong interfacial electric field in lowering reaction barriers. These molecular-level insights into interfacial chemistry not only provide new fundamental understanding of C-F bond activation at the air-water interface but also establish a novel strategy for enhancing nucleophilic reactions in aqueous systems. Furthermore, we successfully translate these principles to practical applications through a scalable reactor design, opening new horizons for addressing persistent environmental contaminants through interface engineering.

### ASSOCIATED CONTENT

### **Data Availability Statement**

All the data supporting the findings of this study are available within the article and its Supporting Information files and from the corresponding author upon reasonable request.

### Supporting Information

The Supporting Information is available free of charge at https://pubs.acs.org/doi/10.1021/acs.est.5c07029.

> Materials list (Text S1); experimental procedures for scale-up reaction settings (Text S2); analytical methods for detection of PFOA, decomposition intermediates, F<sup>-</sup>, Fe(II), O<sub>2</sub><sup>-</sup>, and OH (Text S3); details for stimulated Raman spectroscopy measurements (Text S4); transient absorption spectroscopy measurements (Text S5); Au nanoparticle synthesis (Text S6); interfacial electric field measurements (Text S7); theoretical calculations (Text S8); and additional experimental data in Figures S1-S18 and Tables S1-S2 (PDF)

# AUTHOR INFORMATION

### **Corresponding Author**

Liwu Zhang - Shanghai Key Laboratory of Atmospheric Particle Pollution and Prevention, Department of Environmental Science and Engineering, Fudan University, Shanghai 200433, People's Republic of China; Shanghai Institute of Pollution Control and Ecological Security, Shanghai 200092, People's Republic of China; orcid.org/ 0000-0002-0765-8660; Email: zhanglw@fudan.edu.cn

### **Authors**

Wenbo You - Shanghai Key Laboratory of Atmospheric Particle Pollution and Prevention, Department of Environmental Science and Engineering, Fudan University, Shanghai 200433, People's Republic of China; Shanghai

- Institute of Pollution Control and Ecological Security, Shanghai 200092, People's Republic of China
- **Kejian Li** Shanghai Key Laboratory of Atmospheric Particle Pollution and Prevention, Department of Environmental Science and Engineering, Fudan University, Shanghai 200433, People's Republic of China; Shanghai Institute of Pollution Control and Ecological Security, Shanghai 200092, People's Republic of China; orcid.org/0009-0004-2356-
- Qiuyue Ge Shanghai Key Laboratory of Atmospheric Particle Pollution and Prevention, Department of Environmental Science and Engineering, Fudan University, Shanghai 200433, People's Republic of China
- Yangyang Liu Shanghai Key Laboratory of Atmospheric Particle Pollution and Prevention, Department of Environmental Science and Engineering, Fudan University, Shanghai 200433, People's Republic of China
- Wei Wang Shanghai Key Laboratory of Atmospheric Particle Pollution and Prevention, Department of Environmental Science and Engineering, Fudan University, Shanghai 200433, People's Republic of China
- Haiping Xiong Shanghai Key Laboratory of Atmospheric Particle Pollution and Prevention, Department of Environmental Science and Engineering, Fudan University, Shanghai 200433, People's Republic of China
- Jianpeng Ao State Key Laboratory of Surface Physics, Department of Physics, Fudan University, Shanghai 200433, People's Republic of China
- Jilun Wang Shanghai Key Laboratory of Atmospheric Particle Pollution and Prevention, Department of Environmental Science and Engineering, Fudan University, Shanghai 200433, People's Republic of China
- Le Yang Shanghai Key Laboratory of Atmospheric Particle Pollution and Prevention, Department of Environmental Science and Engineering, Fudan University, Shanghai 200433, People's Republic of China
- Runbo Wang Shanghai Key Laboratory of Atmospheric Particle Pollution and Prevention, Department of Environmental Science and Engineering, Fudan University, Shanghai 200433, People's Republic of China
- Tingting Huang Shanghai Key Laboratory of Atmospheric Particle Pollution and Prevention, Department of Environmental Science and Engineering, Fudan University, Shanghai 200433, People's Republic of China
- Shiyi Wang Beijing Perfectlight Technology Co., Ltd., Beijing 100080, People's Republic of China
- Huan Liu Beijing Perfectlight Technology Co., Ltd., Beijing 100080, People's Republic of China
- Minbiao Ji State Key Laboratory of Surface Physics, Department of Physics, Fudan University, Shanghai 200433, People's Republic of China

Complete contact information is available at: https://pubs.acs.org/10.1021/acs.est.5c07029

### **Author Contributions**

W.Y. and K.L. contributed equally. W.Y.: Writing-original draft, Investigation, Formal analysis, Data curation. K.L.: Writing-review and editing, Investigation, Data curation. Q.G.: Data curation. Y.L.: Data curation. W.W.: Formal analysis, Data curation. H.X.: Validation, Data curation. J.A.: Investigation, Data curation. J.W.: Data curation. L.Y.: Formal analysis. R.W.: Formal analysis. T.H.: Investigation, Data

curation. S.W.: Investigation. Huan Liu: Investigation. M.J.: Supervision. L.Z.: Writing—review and editing, Supervision, Project administration, Investigation, Funding acquisition.

#### Notes

The authors declare no competing financial interest.

### ACKNOWLEDGMENTS

The authors gratefully acknowledge financial support from the National Natural Science Foundation of China (No. 22176036, No. 21976030 and No. 22006020) and the Natural Science Foundation of Shanghai (No. 19ZR1471200).

### REFERENCES

- (1) Cui, J.; Gao, P.; Deng, Y. Destruction of Per- and Polyfluoroalkyl Substances (PFAS) with Advanced Reduction Processes (ARPs): A Critical Review. *Environ. Sci. Technol.* **2020**, *54* (7), 3752–3766.
- (2) Ren, Z.; Bergmann, U.; Leiviskä, T. Reductive degradation of perfluorooctanoic acid in complex water matrices by using the UV/sulfite process. *Water Res.* **2021**, *205*, No. 117676.
- (3) Zhang, H.; Chen, J.-X.; Qu, J.-P.; Kang, Y.-B. Photocatalytic low-temperature defluorination of PFASs. *Nature* **2024**, *635* (8039), *6*10–617.
- (4) DeWitt, J. C. It's too soon to stop studying the potential effects of PFAS on human health. *Nat. Water* **2024**, 2 (8), 700–701.
- (5) Zhang, C.; Tang, T.; Knappe, D. R. U. Oxidation of Per- and Polyfluoroalkyl Ether Acids and Other Per- and Polyfluoroalkyl Substances by Sulfate and Hydroxyl Radicals: Kinetic Insights from Experiments and Models. *Environ. Sci. Technol.* **2023**, *57* (47), 18970–18980.
- (6) Evich, M. G.; Davis, M. J. B.; McCord, J. P.; Acrey, B.; Awkerman, J. A.; Knappe, D. R. U.; Lindstrom, A. B.; Speth, T. F.; Tebes-Stevens, C.; Strynar, M. J.; Wang, Z.; Weber, E. J.; Henderson, W. M.; Washington, J. W. Per- and polyfluoroalkyl substances in the environment. *Science* 2022, 375 (6580), No. eabg9065.
- (7) Gao, J.; Liu, Z.; Chen, Z.; Rao, D.; Che, S.; Gu, C.; Men, Y.; Huang, J.; Liu, J. Photochemical degradation pathways and near-complete defluorination of chlorinated polyfluoroalkyl substances. *Nat. Water* **2023**, *1* (4), 381–390.
- (8) Liu, Z.; Chen, Z.; Gao, J.; Yu, Y.; Men, Y.; Gu, C.; Liu, J. Accelerated Degradation of Perfluorosulfonates and Perfluorocarboxylates by UV/Sulfite + Iodide: Reaction Mechanisms and System Efficiencies. *Environ. Sci. Technol.* **2022**, *56* (6), 3699–3709.
- (9) Schaefer, C. E.; Tran, D.; Fang, Y.; Choi, Y. J.; Higgins, C. P.; Strathmann, T. J. Electrochemical treatment of poly- and perfluor-oalkyl substances in brines. *Environ. Sci.:Water Res. Technol.* **2020**, 6 (10), 2704–2712.
- (10) Guan, Y.; Liu, Z.; Yang, N.; Yang, S.; Quispe-Cardenas, L. E.; Liu, J.; Yang, Y. Near-complete destruction of PFAS in aqueous film-forming foam by integrated photo-electrochemical processes. *Nat. Water* **2024**, 2 (5), 443–452.
- (11) Vecitis, C. D.; Wang, Y.; Cheng, J.; Park, H.; Mader, B. T.; Hoffmann, M. R. Sonochemical degradation of perfluorooctanesulfonate in aqueous film-forming foams. *Environ. Sci. Technol.* **2010**, *44* (1), 432–438.
- (12) Bentel, M. J.; Yu, Y.; Xu, L.; Li, Z.; Wong, B. M.; Men, Y.; Liu, J. Defluorination of Per- and Polyfluoroalkyl Substances (PFASs) with Hydrated Electrons: Structural Dependence and Implications to PFAS Remediation and Management. *Environ. Sci. Technol.* **2019**, *53* (7), 3718–3728.
- (13) Stratton, G. R.; Dai, F.; Bellona, C. L.; Holsen, T. M.; Dickenson, E. R.; Mededovic Thagard, S. Plasma-based water treatment: efficient transformation of perfluoroalkyl substances in prepared solutions and contaminated groundwater. *Environ. Sci. Technol.* 2017, 51 (3), 1643–1648.
- (14) Zhang, Z.; Chen, J.-J.; Lyu, X.-J.; Yin, H.; Sheng, G.-P. Complete mineralization of perfluorooctanoic acid (PFOA) by  $\gamma$ -irradiation in aqueous solution. *Sci. Rep.* **2014**, 4 (1), 7418.

- (15) Javed, H.; Lyu, C.; Sun, R.; Zhang, D.; Alvarez, P. J. J. Discerning the inefficacy of hydroxyl radicals during perfluorooctanoic acid degradation. *Chemosphere* **2020**, 247, No. 125883.
- (16) Li, K.; You, W.; Wang, W.; Gong, K.; Liu, Y.; Wang, L.; Ge, Q.; Ruan, X.; Ao, J.; Ji, M.; Zhang, L. Significantly Accelerated Photochemical Perfluorooctanoic Acid Decomposition at the Air—Water Interface of Microdroplets. *Environ. Sci. Technol.* **2023**, *57* (50), 21448–21458.
- (17) O'Hagan, D. Understanding organofluorine chemistry. An introduction to the C-F bond. *Chem. Soc. Rev.* **2008**, 37 (2), 308–319
- (18) Hayyan, M.; Hashim, M. A.; AlNashef, I. M. Superoxide Ion: Generation and Chemical Implications. *Chem. Rev.* **2016**, *116* (5), 3029–3085.
- (19) Furman, O.; Laine, D. F.; Blumenfeld, A.; Teel, A. L.; Shimizu, K.; Cheng, I. F.; Watts, R. J. Enhanced reactivity of superoxide in water—solid matrices. *Environ. Sci. Technol.* **2009**, *43* (5), 1528–1533.
- (20) Smith, B. A.; Teel, A. L.; Watts, R. J. Identification of the reactive oxygen species responsible for carbon tetrachloride degradation in modified Fenton's systems. *Environ. Sci. Technol.* **2004**, *38* (20), 5465–5469.
- (21) Guo, Y.; Zhang, Y.; Yu, G.; Wang, Y. Revisiting the role of reactive oxygen species for pollutant abatement during catalytic ozonation: The probe approach versus the scavenger approach. *Appl. Catal., B* **2021**, *280*, No. 119418.
- (22) Mitchell, S. M.; Ahmad, M.; Teel, A. L.; Watts, R. J. Degradation of perfluorooctanoic acid by reactive species generated through catalyzed  $\rm H_2O_2$  propagation reactions. *Environ. Sci. Technol. Lett.* **2014**, 1 (1), 117-121.
- (23) Guo, Y.; Zhan, J.; Yu, G.; Wang, Y. Evaluation of the concentration and contribution of superoxide radical for micropollutant abatement during ozonation. *Water Res.* **2021**, *194*, No. 116927.
- (24) Bai, L.; Jiang, Y.; Xia, D.; Wei, Z.; Spinney, R.; Dionysiou, D. D.; Minakata, D.; Xiao, R.; Xie, H.-B.; Chai, L. Mechanistic Understanding of Superoxide Radical-Mediated Degradation of Perfluorocarboxylic Acids. *Environ. Sci. Technol.* **2022**, *56* (1), 624–633
- (25) Javed, H.; Metz, J.; Eraslan, T. C.; Mathieu, J.; Wang, B.; Wu, G.; Tsai, A.-L.; Wong, M. S.; Alvarez, P. J. J. Discerning the Relevance of Superoxide in PFOA Degradation. *Environ. Sci. Technol. Lett.* **2020**, 7 (9), 653–658.
- (26) Halliwell, B.; Gutteridge, J. M. Free radicals in biology and medicine; Oxford University Press: USA, 2015.
- (27) Zheng, J.; Zhang, S. Subnanoscale spatially confined heterogeneous Fenton reaction enables mineralization of perfluor-octanoic acid. *Water Res.* **2023**, 246, No. 120696.
- (28) AlSaleem, S. S.; Zahid, W. M.; Alnashef, I. M.; Haider, H. Destruction of environmentally hazardous halogenated hydrocarbons in stable ionic liquids with superoxide ion radical. *Sep. Purif. Technol.* **2019**, *215*, 134–142.
- (29) Furman, O. S.; Teel, A. L.; Watts, R. J. Volume Reduction of Nonaqueous Media Contaminated with a Highly Halogenated Model Compound Using Superoxide. *J. Agric. Food Chem.* **2010**, 58 (3), 1838–1843.
- (30) Wei, Z.; Li, Y.; Cooks, R. G.; Yan, X. Accelerated Reaction Kinetics in Microdroplets: Overview and Recent Developments. *Annu. Rev. Phys. Chem.* **2020**, 71 (1), 31–51.
- (31) Lee, J. K.; Banerjee, S.; Nam, H. G.; Zare, R. N. Acceleration of reaction in charged microdroplets. *Q. Rev. Biophys.* **2015**, *48* (4), 437–444.
- (32) Lee, J. K.; Kim, S.; Nam, H. G.; Zare, R. N. Microdroplet fusion mass spectrometry for fast reaction kinetics. *Proc. Natl. Acad. Sci. U. S. A.* **2015**, *112* (13), 3898–3903.
- (33) Meng, Y.; Gnanamani, E.; Zare, R. N. Direct C (sp<sup>3</sup>)–N Bond Formation between Toluene and Amine in Water Microdroplets. *J. Am. Chem. Soc.* **2022**, *144* (43), 19709–19713.

- (34) Ruiz-Lopez, M. F.; Francisco, J. S.; Martins-Costa, M. T.; Anglada, J. M. Molecular reactions at aqueous interfaces. *Nat. Rev. Chem.* **2020**, *4* (9), 459–475.
- (35) Kusaka, R.; Nihonyanagi, S.; Tahara, T. The photochemical reaction of phenol becomes ultrafast at the air—water interface. *Nat. Chem.* **2021**, *13* (4), 306–311.
- (36) Fang, Y.-G.; Tang, B.; Yuan, C.; Wan, Z.; Zhao, L.; Zhu, S.; Francisco, J. S.; Zhu, C.; Fang, W.-H. Mechanistic insight into the competition between interfacial and bulk reactions in microdroplets through  $N_2O_5$  ammonolysis and hydrolysis. *Nat. Commun.* **2024**, *15* (1), 2347.
- (37) Xia, D.; Xie, H.-b.; Fu, Z.; Chen, J. Microdroplets: An Overlooked "Engine" of Chemistry in Air. *Environ. Sci. Technol.* **2025**, 59 (13), 6357–6360.
- (38) Martins-Costa, M. T. C.; Anglada, J. M.; Francisco, J. S.; Ruiz-Lopez, M. F. Reactivity of Volatile Organic Compounds at the Surface of a Water Droplet. *J. Am. Chem. Soc.* **2012**, *134* (28), 11821–11827.
- (39) Wood, P. M. The redox potential of the system oxygen—superoxide. Febs Letters 1974, 44 (1), 22–24.
- (40) Martins-Costa, M. T. C.; Anglada, J. M.; Francisco, J. S.; Ruiz-Lopez, M. F. Reactivity of Atmospherically Relevant Small Radicals at the Air–Water Interface. *Angew. Chem., Int. Ed.* **2012**, *51* (22), 5413–5417.
- (41) Björneholm, O.; Hansen, M. H.; Hodgson, A.; Liu, L.-M.; Limmer, D. T.; Michaelides, A.; Pedevilla, P.; Rossmeisl, J.; Shen, H.; Tocci, G. Water at interfaces. *Chem. Rev.* **2016**, *116* (13), 7698–7726.
- (42) Wang, C.; Danovich, D.; Chen, H.; Shaik, S. Oriented External Electric Fields: Tweezers and Catalysts for Reactivity in Halogen-Bond Complexes. J. Am. Chem. Soc. 2019, 141 (17), 7122–7136.
- (43) Li, K.; Gong, K.; Liu, J.; Ohnoutek, L.; Ao, J.; Liu, Y.; Chen, X.; Xu, G.; Ruan, X.; Cheng, H.; Han, J.; Sui, G.; Ji, M.; Valev, V. K.; Zhang, L. Significantly accelerated photochemical and photocatalytic reactions in microdroplets. *Cell Rep. Phys. Sci.* **2022**, 3 (6), No. 100917.
- (44) Li, K.; Ge, Q.; Liu, Y.; Wang, L.; Gong, K.; Liu, J.; Xie, L.; Wang, W.; Ruan, X.; Zhang, L. Highly efficient photocatalytic H<sub>2</sub>O<sub>2</sub> production in microdroplets: accelerated charge separation and transfer at interfaces. *Energy Environ. Sci.* **2023**, *16* (3), 1135–1145.
- (45) Huang, D.; Yin, L.; Niu, J. Photoinduced hydrodefluorination mechanisms of perfluorooctanoic acid by the SiC/graphene catalyst. *Environ. Sci. Technol.* **2016**, *50* (11), 5857–5863.
- (46) Schultz, M. M.; Barofsky, D. F.; Field, J. A. Quantitative Determination of Fluorotelomer Sulfonates in Groundwater by LC MS/MS. *Environ. Sci. Technol.* **2004**, 38 (6), 1828–1835.
- (47) Balmer, M. E.; Sulzberger, B. Atrazine degradation in irradiated iron/oxalate systems: effects of pH and oxalate. *Environ. Sci. Technol.* **1999**, 33 (14), 2418–2424.
- (48) Mulazzani, Q. G.; D'Angelantonio, M.; Venturi, M.; Hoffman, M. Z.; Rodgers, M. A. J. Interaction of formate and oxalate ions with radiation-generated radicals in aqueous solution. Methylviologen as a mechanistic probe. *J. Phys. Chem.* **1986**, *90* (21), 5347–5352.
- (49) Weller, C.; Horn, S.; Herrmann, H. Effects of Fe (III)-concentration, speciation, excitation-wavelength and light intensity on the quantum yield of iron (III)-oxalato complex photolysis. *J. Photochem. Photobiol.*, A 2013, 255, 41–49.
- (50) Bielski, B. H.; Cabelli, D. E.; Arudi, R. L.; Ross, A. B. Reactivity of  $HO_2/O_2^-$  radicals in aqueous solution. *J. Phys. Chem. Ref. Data* **1985**, *14* (4), 1041–1100.
- (51) Hardwick, T. The rate constant of the reaction between ferrous ions and hydrogen peroxide in acid solution. *Can. J. Chem.* **1957**, *35* (5), 428–436.
- (52) Sedlak, D. L.; Hoigné, J. The role of copper and oxalate in the redox cycling of iron in atmospheric waters. *Atmos. Environ. Part A. General Topics* 1993, 27 (14), 2173–2185.
- (53) Kocar, B. D.; Inskeep, W. P. Photochemical Oxidation of As(III) in Ferrioxalate Solutions. *Environ. Sci. Technol.* **2003**, *37* (8), 1581–1588.

- (54) Christensen, H.; Sehested, K. Pulse radiolysis at high temperatures and high pressures. *Radiat. Phys. Chem.* **1981**, *18* (3–4), 723–731.
- (55) Hislop, K. A.; Bolton, J. R. The Photochemical Generation of Hydroxyl Radicals in the UV–vis/Ferrioxalate/H<sub>2</sub>O<sub>2</sub> System. *Environ. Sci. Technol.* **1999**, 33 (18), 3119–3126.
- (56) Pang, H.; Zhang, Q.; Wang, H.; Cai, D.; Ma, Y.; Li, L.; Li, K.; Lu, X.; Chen, H.; Yang, X. Photochemical aging of guaiacol by Fe (III)—oxalate complexes in atmospheric aqueous phase. *Environ. Sci. Technol.* **2018**, 53 (1), 127–136.
- (57) Amii, H.; Uneyama, K. C-F Bond Activation in Organic Synthesis. *Chem. Rev.* **2009**, *109* (5), 2119–2183.
- (58) LaCour, R. A.; Heindel, J. P.; Zhao, R.; Head-Gordon, T. The Role of Interfaces and Charge for Chemical Reactivity in Microdroplets. J. Am. Chem. Soc. 2025, 147 (8), 6299–6317.
- (59) Liu, C.; Li, J.; Chen, H.; Zare, R. N. Scale-up of microdroplet reactions by heated ultrasonic nebulization. *Chem. Sci.* **2019**, *10* (40), 9367–9373.
- (60) Heindel, J. P.; LaCour, R. A.; Head-Gordon, T. The role of charge in microdroplet redox chemistry. *Nat. Commun.* **2024**, *15* (1), 2670
- (61) Liu, Z.; Bentel, M. J.; Yu, Y.; Ren, C.; Gao, J.; Pulikkal, V. F.; Sun, M.; Men, Y.; Liu, J. Near-Quantitative Defluorination of Perfluorinated and Fluorotelomer Carboxylates and Sulfonates with Integrated Oxidation and Reduction. *Environ. Sci. Technol.* **2021**, *55* (10), 7052–7062.
- (62) Zhang, Y.; Liu, J.; Moores, A.; Ghoshal, S. Transformation of 6:2 Fluorotelomer Sulfonate by Cobalt(II)-Activated Peroxymonosulfate. *Environ. Sci. Technol.* **2020**, 54 (7), 4631–4640.
- (63) Zhu, B.; Jiang, W.; Wang, W.; Lin, Y.; Ruan, T.; Jiang, G. Occurrence and Degradation Potential of Fluoroalkylsilane Substances as Precursors of Perfluoroalkyl Carboxylic Acids. *Environ. Sci. Technol.* **2019**, 53 (9), 4823–4831.
- (64) Tang, P.; Jiang, W.; Lyu, S.; Brusseau, M. L.; Xue, Y.; Qiu, Z.; Sui, Q. Mechanism of carbon tetrachloride reduction in ferrous ion activated calcium peroxide system in the presence of methanol. *Chem. Eng. J.* **2019**, 362, 243–250.
- (65) He, X.; Sun, B.; He, M.; Chi, H.; Wang, Z.; Zhang, W.; Ma, J. Highly efficient simultaneous catalytic degradation and defluorination of perfluorooctanoic acid by the  $\rm H_2O_2$ -carbon/MnO<sub>2</sub> system generating  $\rm O_2^-$  and OH synchronously. *Appl. Catal., B* **2020**, 277, No. 119219
- (66) Ogi, Y.; Obara, Y.; Katayama, T.; Suzuki, Y. I.; Liu, S. Y.; Bartlett, N. C. M.; Kurahashi, N.; Karashima, S.; Togashi, T.; Inubushi, Y.; Ogawa, K.; Owada, S.; Rubešová, M.; Yabashi, M.; Misawa, K.; Slavíček, P.; Suzuki, T. Ultraviolet photochemical reaction of  $[Fe(III)(C_2O_4)_3]^{3-}$  in aqueous solutions studied by femtosecond time-resolved X-ray absorption spectroscopy using an X-ray free electron laser. *Struct. Dyn.* **2015**, *2* (3), No. 034901.
- (67) Lee, J. K.; Samanta, D.; Nam, H. G.; Zare, R. N. Micrometersized water droplets induce spontaneous reduction. *J. Am. Chem. Soc.* **2019**, *141* (27), 10585–10589.
- (68) Qiu, L.; Cooks, R. G. Spontaneous Oxidation in Aqueous Microdroplets: Water Radical Cation as Primary Oxidizing Agent. *Angew. Chem., Int. Ed.* **2024**, 63 (17), No. e202400118.
- (69) Liu, G.; Feng, C.; Shao, P. Degradation of Perfluorooctanoic Acid with Hydrated Electron by a Heterogeneous Catalytic System. *Environ. Sci. Technol.* **2022**, *56* (10), 6223–6231.
- (70) Zhou, K.; Su, H.; Gao, J.; Li, H.; Liu, S.; Yi, X.; Zhang, Z.; Wang, W. Deciphering the Kinetics of Spontaneous Generation of  $H_2O_2$  in Individual Water Microdroplets. *J. Am. Chem. Soc.* **2024**, *146* (4), 2445–2451.
- (71) Jonah, C. D.; Miller, J. R.; Matheson, M. S. The reaction of the precursor of the hydrated electron with electron scavengers. *J. Phys. Chem.* **1977**, *81* (17), 1618–1622.
- (72) Buxton, G. V.; Greenstock, C. L.; Helman, W. P.; Ross, A. B. Critical review of rate constants for reacitons of hydrated electrons. *J. Phys. Chem. Ref. Data* **1988**, *17* (2), 513–886.

- (73) Huang, L.; Dong, W.; Hou, H. Investigation of the reactivity of hydrated electron toward perfluorinated carboxylates by laser flash photolysis. *Chem. Phys. Lett.* **2007**, 436 (1), 124–128.
- (74) Banayan Esfahani, E.; Asadi Zeidabadi, F.; Zhang, S.; Mohseni, M. Photo-chemical/catalytic oxidative/reductive decomposition of per- and poly-fluoroalkyl substances (PFAS), decomposition mechanisms and effects of key factors: a review. *Environ. Sci.:Water Res. Technol.* 2022, 8 (4), 698–728.
- (75) Moorhead, E. G.; Sutin, N. Rate and Equilibrium Constants for the Formation of the Monooxalate Complex of Iron(III). *Inorg. Chem.* **1966**, 5 (11), 1866–1871.
- (76) Lee, Y.-C.; Wang, P.-Y.; Lo, S.-L.; Huang, C. P. Recovery of perfluorooctane sulfonate (PFOS) and perfluorooctanoate (PFOA) from dilute water solution by foam flotation. *Sep. Purif. Technol.* **2017**, 173, 280–285.
- (77) Armstrong, D. A.; Huie, R. E.; Koppenol, W. H.; Lymar, S. V.; Merényi, G.; Neta, P.; Ruscic, B.; Stanbury, D. M.; Steenken, S.; Wardman, P. Standard electrode potentials involving radicals in aqueous solution: inorganic radicals (IUPAC Technical Report). *Pure Appl. Chem.* **2015**, *87* (11–12), 1139–1150.
- (78) Gonzalez, M. C.; Le Roux, G. C.; Rosso, J. A.; Braun, A. M. Mineralization of CCl<sub>4</sub> by the UVC-photolysis of hydrogen peroxide in the presence of methanol. *Chemosphere* **2007**, *69* (8), 1238–1244.
- (79) Wang, Y.; Zhang, J.; Zhang, W.; Yao, J.; Liu, J.; He, H.; Gu, C.; Gao, G.; Jin, X. Electrostatic Field in Contact-Electro-Catalysis Driven C–F Bond Cleavage of Perfluoroalkyl Substances. *Angew. Chem., Int. Ed.* **2024**, 63 (19), No. e202402440.
- (80) Bach, R. D.; Ayala, P. Y.; Schlegel, H. B. A Reassessment of the Bond Dissociation Energies of Peroxides. An ab Initio Study. *J. Am. Chem. Soc.* **1996**, *118* (50), 12758–12765.
- (81) Singh, A. Chemical and biochemical aspects of superoxide radicals and related species of activated oxygen. *Can. J. Physiol. Pharmacol.* **1982**, *60* (11), 1330–1345.
- (82) Biswas, S.; Yamijala, S. S. R. K. C.; Wong, B. M. Degradation of Per- and Polyfluoroalkyl Substances with Hydrated Electrons: A New Mechanism from First-Principles Calculations. *Environ. Sci. Technol.* **2022**, *56* (12), 8167–8175.
- (83) Wang, Y.; Zhang, P. Photocatalytic decomposition of perfluorooctanoic acid (PFOA) by TiO<sub>2</sub> in the presence of oxalic acid. *J. Hazard. Mater.* **2011**, *192* (3), 1869–1875.
- (84) Xia, D.; Zhang, H.; Ju, Y.; Xie, H.-b.; Su, L.; Ma, F.; Jiang, J.; Chen, J.; Francisco, J. S. Spontaneous Degradation of the "Forever Chemicals" Perfluoroalkyl and Polyfluoroalkyl Substances (PFASs) on Water Droplet Surfaces. *J. Am. Chem. Soc.* **2024**, *146* (16), 11266–11271.
- (85) Costanza, J.; Arshadi, M.; Abriola, L. M.; Pennell, K. D. Accumulation of PFOA and PFOS at the Air—Water Interface. *Environ. Sci. Technol. Lett.* **2019**, *6* (8), 487–491.
- (86) Li, R.; Isowamwen, O. F.; Ross, K. C.; Holsen, T. M.; Thagard, S. M. PFAS—CTAB Complexation and Its Role on the Removal of PFAS from a Lab-Prepared Water and a Reverse Osmosis Reject Water Using a Plasma Reactor. *Environ. Sci. Technol.* **2023**, *57* (34), 12901—12910.
- (87) Jungwirth, P.; Tobias, D. J. Ions at the Air/Water Interface. J. Phys. Chem. B **2002**, 106 (25), 6361–6373.
- (88) Jungwirth, P.; Tobias, D. J. Specific Ion Effects at the Air/Water Interface. Chem. Rev. 2006, 106 (4), 1259–1281.
- (89) Benjamin, I. Chemical Reactions and Solvation at Liquid Interfaces: A Microscopic Perspective. *Chem. Rev.* **1996**, *96* (4), 1449–1476.
- (90) Wang, D.; Zhao, L.; Wang, D.; Yan, L.; Jing, C.; Zhang, H.; Guo, L.-H.; Tang, N. Direct evidence for surface long-lived superoxide radicals photo-generated in TiO2 and other metal oxide suspensions. *Phys. Chem. Chem. Phys.* **2018**, 20 (28), 18978–18985.
- (91) Wang, L.; Li, K.; Liu, Y.; Gong, K.; Liu, J.; Ao, J.; Ge, Q.; Wang, W.; Ji, M.; Zhang, L. Significantly Accelerated Hydroxyl Radical Generation by Fe(III)—Oxalate Photochemistry in Aerosol Droplets. *J. Phys. Chem. A* **2023**, 127 (1), 250–260.

- (92) Martins-Costa, M. T. C.; Ruiz-López, M. F. Electrostatics and Chemical Reactivity at the Air-Water Interface. *J. Am. Chem. Soc.* **2023**, *145* (2), 1400–1406.
- (93) Sen, S.; Yamaguchi, S.; Tahara, T. Different Molecules Experience Different Polarities at the Air/Water Interface. *Angew. Chem., Int. Ed.* **2009**, 48 (35), 6439–6442.
- (94) Rai, P. K.; Kumar, A.; Kumar, P. Spontaneous Deprotonation of HO2• at Air-Water Interface. *J. Phys. Chem. A* **2025**, 129 (12), 2912–2921.
- (95) Lee, J. K.; Samanta, D.; Nam, H. G.; Zare, R. N. Spontaneous formation of gold nanostructures in aqueous microdroplets. *Nat. Commun.* **2018**, *9* (1), 1562.
- (96) Kathmann, S. M.; Kuo, I. F. W.; Mundy, C. J. Electronic Effects on the Surface Potential at the Vapor-Liquid Interface of Water. J. Am. Chem. Soc. 2008, 130 (49), 16556-16561.
- (97) Shi, L.; LaCour, R. A.; Qian, N.; Heindel, J. P.; Lang, X.; Zhao, R.; Head-Gordon, T.; Min, W. Water structure and electric fields at the interface of oil droplets. *Nature* **2025**, *640* (8057), 87–93.
- (98) Fumagalli, L.; Esfandiar, A.; Fabregas, R.; Hu, S.; Ares, P.; Janardanan, A.; Yang, Q.; Radha, B.; Taniguchi, T.; Watanabe, K.; Gomila, G.; Novoselov, K. S.; Geim, A. K. Anomalously low dielectric constant of confined water. *Science* **2018**, *360* (6395), 1339–1342.
- (99) Shaik, S.; Ramanan, R.; Danovich, D.; Mandal, D. Structure and reactivity/selectivity control by oriented-external electric fields. *Chem. Soc. Rev.* **2018**, *47* (14), 5125–5145.
- (100) Fried, S. D.; Boxer, S. G. Measuring electric fields and noncovalent interactions using the vibrational Stark effect. *Acc. Chem. Res.* **2015**, 48 (4), 998–1006.
- (101) Xiong, H.; Lee, J. K.; Zare, R. N.; Min, W. Strong electric field observed at the interface of aqueous microdroplets. *J. Phys. Chem. Lett.* **2020**, *11* (17), 7423–7428.
- (102) Fang, Y.; Li, X.; Yuan, C.; Li, X.; Yuan, X.; Zhang, D.; Zhang, X.; Zhu, C.; Fang, W. Spontaneous Generation of Alkoxide Radical from Alcohols on Microdroplets Surface. *Angew. Chem., Int. Ed.* **2025**, 64 (6), No. e202417920.
- (103) Oklejas, V.; Sjostrom, C.; Harris, J. M. SERS Detection of the Vibrational Stark Effect from Nitrile-Terminated SAMs to Probe Electric Fields in the Diffuse Double-Layer. *J. Am. Chem. Soc.* **2002**, 124 (11), 2408–2409.
- (104) Joy, J.; Stuyver, T.; Shaik, S. Oriented External Electric Fields and Ionic Additives Elicit Catalysis and Mechanistic Crossover in Oxidative Addition Reactions. *J. Am. Chem. Soc.* **2020**, 142 (8), 3836–3850.
- (105) Sun, A.; Lankin, D. C.; Hardcastle, K.; Snyder, J. P. 3-Fluoropiperidines and N-methyl-3-fluoropiperidinium salts: The persistence of axial fluorine. *Chem.—Eur. J.* **2005**, *11* (5), 1579–1591.
- (106) Hao, H.; Leven, I.; Head-Gordon, T. Can electric fields drive chemistry for an aqueous microdroplet? *Nat. Commun.* **2022**, *13* (1), 280
- (107) Laidler, K. J.; Keith, J. Chemical kinetics; McGraw-Hill: New York, 1965; 2.